Chemosphere 335 (2023) 139093

Contents lists available at ScienceDirect

Chemosphere

journal homepage: www.elsevier.com/locate/chemosphere

Mechanistic investigation of direct photodegradation of chloroquine phosphate under simulated sunlight

Weiming Xiang [a], Fahao Xu [a], Dong Wan [b], Xing Wang [a], Fan Luo [a,**], Yong Chen [a,*]

[a] School of Environmental Science and Engineering, Huazhong University of Science and Technology, Wuhan, 430074, PR China
[b] Institute of Hydrobiology, Chinese Academy of Sciences, Wuhan, 430072, PR China

HIGHLIGHTS

- High pH value and low initial concentration accelerated the CQ degradation.
- The ^{3}CQ* played the dominant role during direct photodegradation.
- The CQ photodegradation pathway was proposed by HPLC-MS/MS.
- The photodegradation involved dechlorination and substitution of the hydroxyl group.
- The energy barrier of dichlorination process was calculated by DFT calculation.

GRAPHICAL ABSTRACT

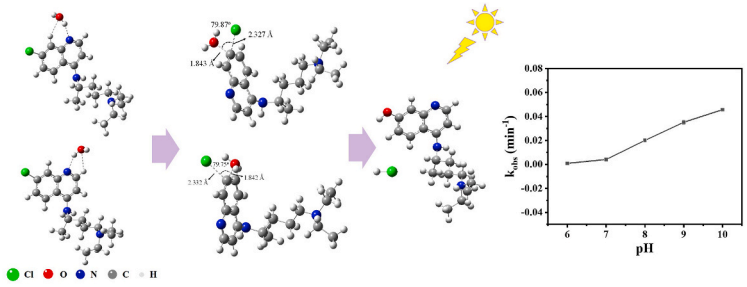

ARTICLE INFO

Handling Editor: Keith Maruya

Keywords:
Chloroquine phosphate
Direct photodegradation
Simulated sunlight
Energy barrier
Photodegradation pathway

ABSTRACT

Chloroquine phosphate (CQ) is an antiviral drug for Coronavirus Disease 2019 and an old drug for treatment of malaria, which has been detected in natural waters. Despite its prevalence, the environmental fate of CQ remains unclear. In this study, the direct photodegradation of CQ under simulated sunlight was investigated. The effect of various parameters such as pH, initial concentration and environmental matrix were examined. The photodegradation quantum yield of CQ (4.5×10^{-5}–0.025) increased with the increasing pH value in the range of 6.0–10.0. The electron spin resonance (ESR) spectrometry and quenching experiments verified that the direct photodegradation of CQ was primarily associated with excited triplet states of CQ (^{3}CQ*). The common ions had negligible effect and humic substances exhibited a negative effect on CQ photodegradation. The photoproducts were identified using high-resolution mass spectrometry and the photodegradation pathway of CQ was proposed. The direct photodegradation of CQ involved the cleavage of the C–Cl bond and substitution of the hydroxyl group, followed by further oxidation to yield carboxylic products. The photodegradation processes were further confirmed by the density functional theory (DFT) computation for the energy barrier of CQ dichlorination. The findings contribute to the assessment of the ecological risk associated with the overuse of Coronavirus drugs during global public health emergencies.

* Corresponding author.
** Corresponding author.
E-mail addresses: fl4021@hust.edu.cn (F. Luo), ychen@hust.edu.cn (Y. Chen).

https://doi.org/10.1016/j.chemosphere.2023.139093
Received 22 February 2023; Received in revised form 19 May 2023; Accepted 30 May 2023
Available online 31 May 2023

Credit authors statement

Weiming Xiang: Conceptualization, methodology, investigation, writing - original draft, validation, formal analysis, visualization, software. Fahao Xu: Data curation, investigation, software. Dong Wan: writing - review & editing, funding acquisition. Xing Wang: Data curation. Luo Fan: Review & editing, validation. Yong Chen: Resources, writing - review & editing, funding acquisition.

1. Introduction

The COVID-19 pandemic has spread rapidly around the world in December 2019, causing serious impacts on both human health and the global economy (Zhao et al., 2020). Chloroquine phosphate (CQ), an old drug for treatment of malaria, was an effective drug for treating COVID-19 (Gao et al., 2020; Wang et al., 2020; Sulistyaningrum et al., 2020). Consequently, CQ has been used in the therapeutic processes and subsequently released into the environment through medical wastewater emissions since it is incompletely absorbed by the human body (Du and Chen, 2020; Simani et al., 2021; Yao et al., 2020). The CQ release could pose a potential ecological risk to both animal and human health. Therefore, it is essential to understand the fate of CQ in natural waters.

Photodegradation is the primary elimination process of organic pollutants in natural waters under solar irradiation. Direct photodegradation occurs when the absorption spectra of organic pollutants overlap with the emission spectrum of terrestrial sunlight. Given that the CQ molecule has considerable sunlight absorption in the wavelength range of 290–360 nm, it can be activated to its excited singlet state (^{1}CQ*) under sunlight irradiation (Gaigalas et al., 2004). Subsequently, the excited triplet states of CQ (^{3}CQ*) are formed through intersystem crossing (ISC), which is unstable and readily decomposed, leading to the direct photodegradation. For instance, direct photodegradation dominated the photochemical processes of metoclopramide and chlortetracycline (Chen et al., 2012; Dabic et al., 2022) and the direct photodegradation processes depend on chemical structures of the organic pollutants (Chen et al., 2000, 2001a, 2001b). Additionally, the excited state CQ molecular (^{1}CQ*, ^{3}CQ*) could produce reactive oxygen species (ROS, such as hydroxyl radical ($HO^\bullet$) and singlet oxygen ($^1O_2$)), which could lead to the self-sensitized oxidation of organic pollutants in the aquatic environment by analogy with fluoroquinolone antibiotic (Ge et al., 2010) and p-aminobenzoic acid (Zhang et al., 2016). Thus, it is essential to investigate the generation of ^{3}CQ*, $HO^\bullet$ and $^1O_2$ during the irradiation to explore the mechanism of CQ photodegradation.

Dissolved organic matters (DOM), including humic acid (HA) and fulvic acid (FA), are ubiquitous in aquatic environment and can absorb solar irradiation to form the excited triplet state of DOM (^{3}DOM*) (Janssen et al., 2014; Makunina et al., 2015; Chen et al., 2017) and ROS ($HO^\bullet$, $^1O_2$) (Mathon et al., 2019; Cheng et al., 2023). It is widely reported that DOM plays dual roles for the photodegradation of organic pollutants in natural waters (Redman et al., 2021; Zhang et al., 2019a). ^{3}DOM* and ROS lead to photosensitization degradation of pollutants, while the inner-filter of DOM acts as light-screening effect (Bai et al., 2021; Boreen et al., 2008; Wenk et al., 2011; Zhou et al., 2013). Additionally, the coexistent ions in the natural waters may affect the direct photodegradation of organic pollutants (Wang et al., 2015). Therefore, the effect of DOM in different water matrices on the photodegradation process of CQ needed to be investigated.

The overall objective of this study was to investigate the direct photodegradation mechanism of CQ and the effect of environmental matrix on CQ photodegradation. The roles of ^{3}CQ*, $HO^\bullet$ and $^1O_2$ was examined using chemical probes and electron spin resonance (ESR) spectrometry. The major photodegradation products of CQ was identified through high-resolution mass spectrometry. The toxicity of photoproducts in direct photodegradation of CQ was evaluated. The degradation pathway was proposed according to the photoproducts and energy barrier model of CQ via DFT calculation.

2. Material and methods

2.1. Material and reagents

Chloroquine phosphate (>98%) was purchased from Shanghai Lianshuo Biological Technology Co, Ltd. The humic acid (HA) and fulvic acid (FA) were obtained from Sigma-Aldrich and Henan Changsheng Science Company, respectively. Methanol and acetonitrile were purchased from Merck. All chemicals used were of at least analytical reagent grade. Ultra-pure water with a resistivity of 18.25 MΩ cm was used in the whole experimental process.

2.2. Photodegradation experiments

The direct photodegradation experiment was performed using a temperature controlled photodegradation device equipped with a 150 W xenon lamp and a <300 nm cutoff filter, which is depicted in Schematic S1 of Supporting Information. The emission spectrum of the light source is shown in Fig. S1. The total photon irradiance in the range of 290–380 nm ($E^0_{p,\ tot}$, 1.51×10^{-8}, Einstein·cm^{-2} s^{-1}) was determined and calculated by a p-nitroanisole/pyridine (PNA/PYR) actinometer (See Text S1 for details). The CQ stock solution was dispersed in phosphate buffered solutions (5.0 mM) at various pH values (6.0−10.0) with a total solution volume of 20.0 mL in the quartz reactor. The irradiation source was then opened for 30 min before experiments. 200 μL aliquots of samples (1.0 ml in all for sampling 5 times) were withdrawn at various intervals and substrate decay was measured by HPLC. The pseudo-first-order reaction rate constants (k_{obs}) and half-lifetime ($t_{1/2}$) of CQ photodegradation were calculated as described in Text S2.

2.3. Analytical methods

The concentration of CQ was determined using an Agilent 1260 HPLC system equipped with a C18 reverse phase column (Agilent Technologies, 350 mm × 4.6 mm, 5 μm) and a DAD detector set at 329 nm. The mobile phase consisted of acetonitrile (phase A) and 0.01 M KH_2PO_4 solution (pH = 2.5, phase B) with ratio of 18/82. The column temperature was set to 30 °C, the flow rate was 1.0 mL min^{-1} and the injection volume was 20 μL.

The degradation products of CQ were identified using liquid chromatography high-resolution mass spectrometry (Agilent LC/MS D1100 Q Exactive Orbitrap) with an UltiMate 3000 HPLC and Hypersil GOLD C18 phase column (100 mm × 2.1 mm, 3 μm). The mobile phase was water (0.1% formic acid) and acetonitrile (0.1% formic acid) at a flow rate of 0.2 mL min^{-1}. The sample was gradient eluted with 10% acetonitrile. Subsequently, the acetonitrile linearly increased to 70% in 10 min and then recovered to 10% in another 10 min. The injection volume was 30 μL. The ESI source parameters were as follows: spraying voltage 3200 V, capillary temperature 300 °C, sheath gas 40, probe heater 350 °C.

2.4. Mechanism analysis

ESR spectra were obtained from solution samples (100 mM) using 1−20 mW microwave power and 100 kHz field modulation with the amplitude set to 1 G, using dimethyl pyridine N-oxide (DMPO) and 2,2,6,6-tetramethylpiperidine-1-oxyl (TMPO) supplied by Aladdin as spin trappers (100.0 mM) for $HO^\bullet$ and $^1O_2$, respectively. The light source was 200 W xenon light. The g-values for each ESR spectrum were extracted from simulations performed using Easyspin (v5.2.23). For the experiment, 10.0 mg CQ dispersed in 5.0 mL water. After ultrasonic vibration, 100 μL DMPO/TMPO solution (100 mM) was added into 200 μL sample. The mixed solution was taken into the capillary for the measure of reactive species.

The quantum mechanical calculation was carried out based on the density functional theory (DFT) method using the Gaussian 09 W. The CQ molecular was optimizedunder the B3LYP/6-311G + (2d, p) and the energy point was computed under M06-2X/6-311G + (2d, p). Besides, the energy was calculated with the Solvation Model based on Density (SMD). The energy of special photoproducts was calculated and the barrier of energy was depicted.

3. Results and discussion

3.1. Direct photodegradation of CQ

The absorption capacity of simulated sunlight by CQ was evaluated using the UV–vis absorption method and the quantum yield was calculated as described in Text S3. Fig. 1 shows the UV–vis absorbance spectra of CQ (pKa = 8.4 (Yi et al., 2021)) at pH values range of 6.0–10.0 with a primary absorption peak around 340 nm. The spectra overlap between the light absorption of CQ (Fig. 1) and simulated sunlight (Fig. S1) could lead to the direct photodegradation of CQ. Fig. S2 illustrated that rapid degradation of CQ occurred upon irradiation under simulated sunlight. As shown in Fig. 1, the absorbance of CQ at 342 nm decreased with increasing pH, which was likely attributed to the increasing proportions of deprotonated forms of CQ. Since the pKa value of CQ is 8.4, the deprotonated forms increased gradually from pH 6.4 until nearly full deprotonation at pH 10.4 in the aqueous solution. Accordingly, the deprotonated form of CQ exhibits a weaker light absorption under simulated sunlight.

Fig. S3 illustrates the degradation kinetics of CQ at different pH values and initial concentration. The values of $t_{1/2}$ and k_{obs} for CQ photodegradation were calculated and presented in Table S1 and Table S2. The k_{obs} (0.0026−0.027 min^{-1}) of CQ direct photodegradation decreased with the increase of its initial concentration (10.0−80.0 μM) in Fig. S3(a). As shown in Fig. S3(b), the k_{obs} (0.0095−0.046 min^{-1}) of CQ increased with increasing pH values in the range of 6.0–10.0. Furthermore, the quantum yield of CQ was found to increase from 4.5 × 10^{-5} at pH 6.0 to 0.025 at pH 10.0. The quantum yield of CQ increased markedly at higher pH values, which is corresponding to the higher proportion of deprotonated forms of CQ (Fig. 2). Accordingly, the deprotonation process of CQ facilitated direct photodegradation under simulated sunlight. The influence of temperature (20−35 °C) on CQ photodegradation was shown in Fig. S4. The CQ photodegradation efficiency increased with increasing temperature. It is likely due to the higher generated rate of ^{3}CQ* molecules at high temperature, resulting in more rapid direct photodegradation of CQ.

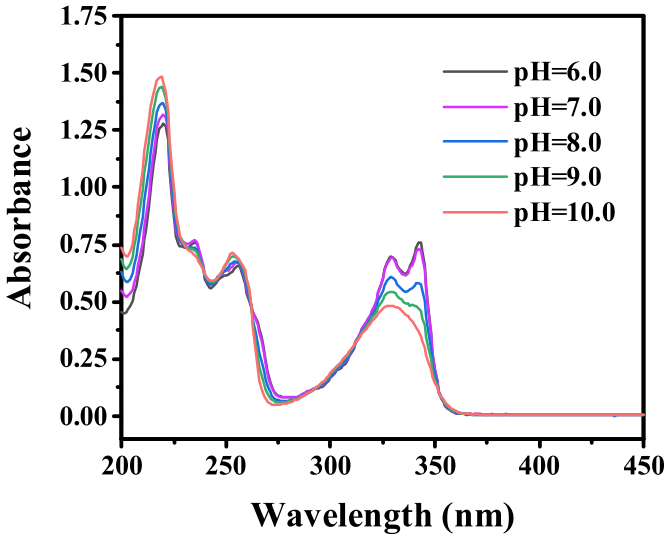

Fig. 1. The UV–vis absorption spectra in 200–450 nm wavelength of CQ.

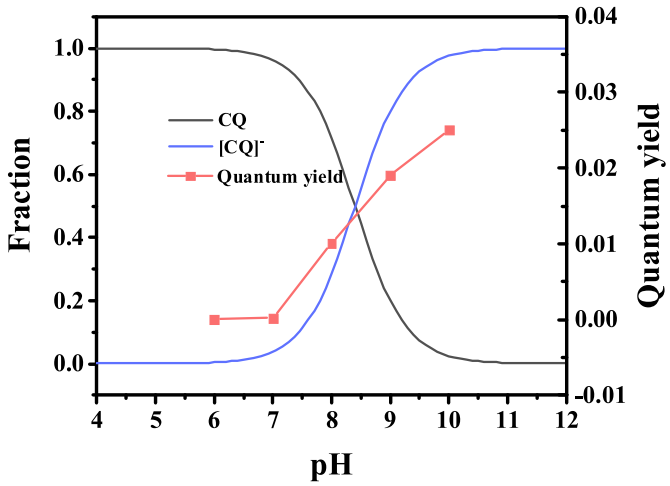

Fig. 2. The existence form and photodegradation quantum yield of CQ (20.0 μM) at different pH.

3.2. Effect of environmental matrix on the photodegradation of CQ

Humic substances are ubiquitous in natural water systems and can have a significant impact on the photodegradation of CQ. Fig. S5(a) shows the effect of FA and HA (5 mg L^{-1}) on the photodegradation of CQ at different pH values. The k_{obs} values and $t_{1/2}$ are listed in Table S3. It can be found that increasing pH values accelerated the photodegradation of CQ in all cases. The addition of FA exhibited a noticeable inhibition effect on CQ degradation, while the presence of HA had little effect on the k_{obs} values. Since the HS solutions had absorbance at λ > 300 nm (Fig. S5(b)), HS could act as both a photosensitizer and a light screener for the photodegradation of CQ. The total light-screening factor ($\hat{S}$) of HS was calculated as described in Text S4. The $\hat{S}$ of HA and FA were calculated to be 0.92, 0.92, 0.92, 0.91, 0.89 and 0.74, 0.74, 0.72, 0.71, 0.71 at pH values of 6.0, 7.0, 8.0, 9.0 and 10.0, respectively. The high $\hat{S}$ value of HA, which was close to 1, suggested that HA had little effect on CQ photodegradation, while FA acted as a light screener for the photodegradation of CQ.

The photodegradation of CQ was also tested in different natural waters matrices, such as lake and river waters, as well as effluent organic matter (EfOM) solutions. The natural waters were collected from Yangtze River, East Lake and Yujia Lake in Wuhan, China. Fig. S6(a) shows the photodegradation kinetics of CQ in different water matrices and the values of k_{obs} and $t_{1/2}$ are listed in Table S4. The results show that the photodegradation of CQ was significantly inhibited in the Yujia Lake water and EfOM solution, while the other two natural waters had little effect on the photodegradation. This inhibition was attributed to the light screening effect of the Yujia Lake water and EfOM solution, which had strong absorbance at λ > 300 nm (Fig. S6(b)). The phenomenon was correlated with the presence of HA and FA (Kulovaara et al., 1996). In addition, the influence of common cations (Mn^{2+}, Mg^{2+}, Ca^{2+}, and Fe^{3+}) and anions (HCO_3^-, NO_3^-, SO_4^{2-}, and Cl^-) on the photodegradation of CQ was depicted in Fig. S7. The addition of these cations and anions had little impact on the CQ photodegradation.

3.3. Effect of ROS on photodegradation

By analogy with other compounds, the effect of dissolved oxygen (DO) on CQ photodegradation was investigated under constant N_2 or O_2 purging (Song et al., 1998; Zhang et al., 2019b). Fig. 3 illustrated that the photodegradation of CQ was promoted by purging with N_2, but inhibited by purging with O_2, compared to the experiments in air. The k_{obs} of CQ photodegradation was 0.0091, 0.0066 and 0.0075 min^{-1} in N_2, O_2, and pure CQ, respectively. CQ could undergo direct and self-sensitized photodegradation like the fluoroquinolones

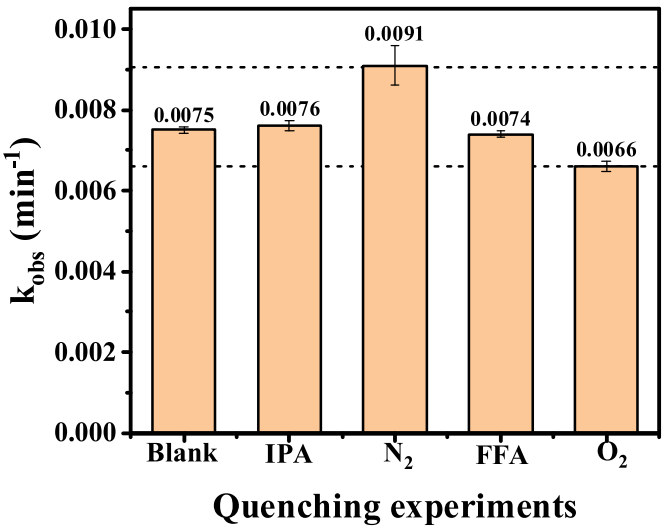

Fig. 3. The k_{obs} of CQ in the reactive species quenching experiments ($[IPA]_0$ = 10.0 mM, $[FFA]_0$ = 200 μM, O_2 and N_2 saturated 30 min, $[CQ]_0$ = 20.0 μM, pH = 8.0, T = 25 °C).

photodegradation process (Albini and Monti, 2003). The possible reactions were as follows:

$$CQ + hv \rightarrow {}^1CQ^* \quad (1)$$

$${}^1CQ^* \rightarrow {}^3CQ^* \quad (2)$$

$${}^3CQ^* \rightarrow \text{product} \quad (3)$$

$${}^3CQ^* + {}^3O_2 \rightarrow CQ + {}^1O_2 \quad (4)$$

$${}^3CQ^* + {}^3O_2 \rightarrow O_2^{\bullet-} + CQ^{\bullet+} \quad (5)$$

Upon excitation by irradiation absorption, the ground state of CQ was excited to $^1CQ^*$ and then underwent ISC to generate $^3CQ^*$. $^3CQ^*$ and $^1CQ^*$ was quenched by $^3O_2$, leading to the formation of $^1O_2$ and superoxide radical ($O_2^{\bullet-}$). $O_2^{\bullet-}$ readily dismutates into O_2 and H_2O_2, which can be converted into $HO^\bullet$ under sunlight irradiation. Thus, the reaction mechanism between CQ and $^1O_2$, or $HO^\bullet$ needed to be elucidated. Isopropanol (IPA) and furfuryl alcohol (FFA) was used as quenchers of $HO^\bullet$ and $^1O_2$, respectively (Bwab et al., Lm; Yu et al., 2015). As shown in Fig. 3, the CQ photodegradation degradation was fitted by first-order kinetic process. The k_{obs} of CQ in absence and presence of IPA and FFA were 0.0075, 0.0076, 0.0074 min^{-1}, respectively, indicating that $HO^\bullet$ and $^1O_2$ had little contribution to the CQ photodegradation. Accordingly, the direct photodegradation of $^3CQ^*$ played a significant role in CQ degradation. Fig. 4(a) indicated that the ESR spectrum of $HO^\bullet$ was weak during the photodegradation of CQ, which further confirmed that $HO^\bullet$ had little impact on CQ photodegradation. As shown in Fig. 4 (b), the ESR spectrum of $^1O_2$ exhibited increasing signal intensity with time. Nevertheless, the FFA had no effect on CQ photodegradation (Fig. 3), indicating $^1O_2$ played a negligible role in the photodegradation. To further investigate the specific influence of the reactive species ($^1O_2$, $^3CQ^*$, and $HO^\bullet$) in the CQ photodegradation process, probe experiments were also conducted using FFA, 2,4,6-trimethylphenol (TMP) and terephthalate (TPA) (Bwab et al., Lm; Remke et al., 2022; Snyrychova and Hideg, 2007).

The elimination and production of FFA, TMP and H-TPA are presented in Figs. S8(a and b), and the monitoring methods for FFA, TMP and H-TPA are provided in Text S5 (Wan et al., 2022a). The efficiency of FFA and TMP degradation was found to be 6.2% and 69.6%, respectively, and the results demonstrate the absence of H-TPA production, which is consistent with the quenching experiment and ESR detection. To further explore the mechanism of CQ photodegradation, the

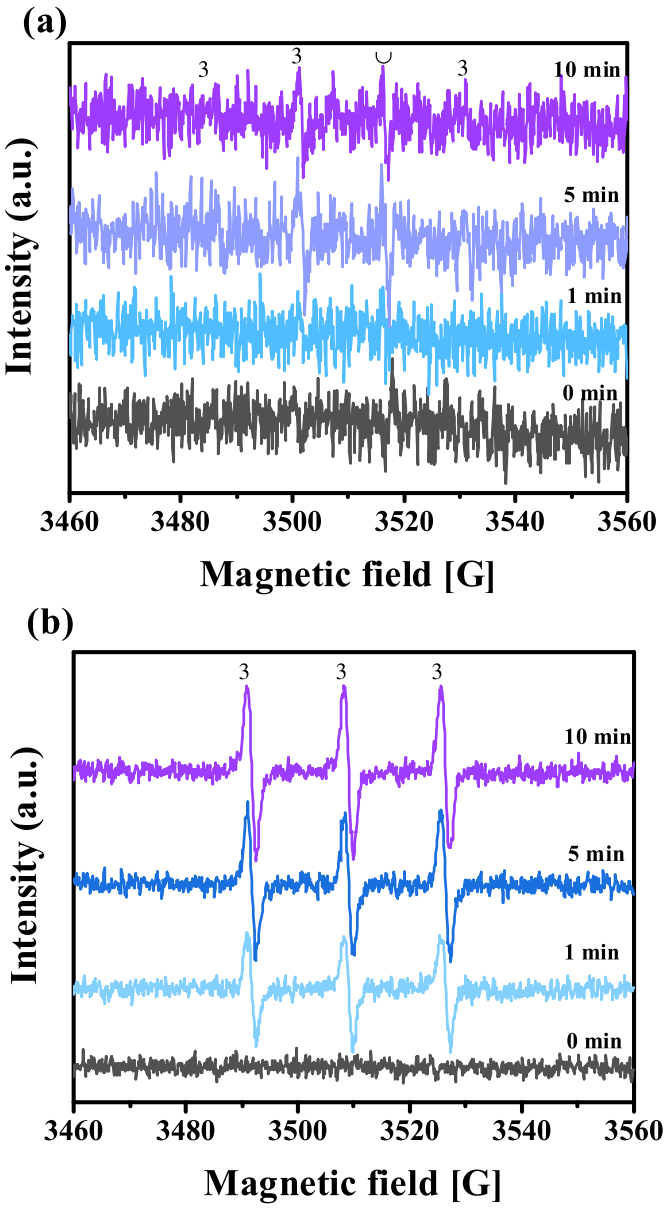

Fig. 4. The ESR spectra of (a) $HO^\bullet$ and (b) $^1O_2$.

competition experiment of FFA and CQ was conducted using Rose Bengal (RB) under simulated sunlight irradiation. The light source bellow 400 nm or 380 was removed by the filter, respectively. The degradation efficiency of CQ and FFA was shown in Fig. S9 (Wan et al., 2022b). The FFA degradation efficiency was 6.2%, 7.2% and 7.3% in the systems of CQ/FFA/RB/400 nm, CQ/FFA/RB/380 nm and FFA/RB/400 nm, respectively, indicating that CQ was hardly reacted with the $^1O_2$. Figs. S10(a and b) shows that the degradation of TMP under simulated sunlight. In Fig. S10(a), the TMP was degraded under different conditions, including TMP/CQ/IPA, TMP/IPA, pure TMP and TMP/CQ. The TMP degradation efficiency was higher when CQ was present in the system (15.0% and 15.7% for TMP/CQ/IPA and TMP/CQ, respectively) compared to pure TMP and TMP/IPA (8.1% and 9.5%, respectively). Therefore, CQ exhibited an accelerating effect on TMP degradation upon irradiation, indicating that the formation of $^3CQ^*$ which was responsible for direct photodegradation of CQ. Moreover, the kinetic calculation of TMP degradation is depicted in Fig. S10(b), where first-order kinetic were used to fit the data. The k_{obs} was ≈0.002 min^{-1} with CQ, which was higher than that in the pure TMP photodegradation process (≈0.001 min^{-1}). The kinetic constant supports that the $^3CQ^*$ direct degradation

plays an essential role in the CQ photodegradation process.

3.4. The photoproducts and toxicity of CQ

The HPLC-MS/MS technique was employed to determine the direct photodegradation products of CQ. Fig. S11 shows the total ion current chromatogram of the main photoproducts (C1–C3, C5–C6). The possible pathways of CQ degradation are displayed in Fig. 5. The first-order and second-order mass spectrometry of C1–C3 and C5–C6 are shown in Fig. S12. During the photodegradation process, the -Cl connected moiety attached to the benzene ring was substituted by –OH originating from H_2O (Albini and Monti, 2003; Anaya-Gonzalez et al., 2019). Specifically, the -Cl connected on the benzene ring was substituted by –OH, which was from the H_2O molecular. In the reaction, the C1 was transformed into C2. Then, C2 had the other reacted pathway to form the molecular C3, which took off the $–CH_2CH_3$. In addition, the –OH substituted the –H on the ortho-carbon from C2 under the irradiation and C4 was formed. However, C4 was unstable and the –OH on two ortho-carbons of C4 were immediately dehydrated to form the –COOH of C5 and then the C5 occurred decarboxylation and hydroxyl substitution reactions to form the C6. Besides, the relative toxicity of photoproducts was assessed based on the decrease of the luminescence emitted by *Vibrio fischeri*. The method is described in Text S6 and the relative inhibition ratio is shown in Fig. 6. The inhibition ratio was 45.3% at 20 min, which elicited high toxicity towards the *Vibrio fischeri*. Generally, the relative toxicity of the CQ photodegradation process increased during CQ photodegradation process, which was attributed to the different photoproduct formation.

3.5. Density functional theory calculations

The DFT calculation was employed to predict the probability of CQ molecule deactivation process. During the photodegradation CQ, the chlorine (-Cl) linked to the benzene ring was activated by solar irradiation and the initial reaction played the dominant role in the process. The transition states (TS1, TS2) were selected and optimized using the basic set under B3LYP/6–31 + g (d, p). The structures of TS1 and TS2 were presented in Fig. S13 (a, c) and the atomic Cartesian coordinates of the TS1 and TS2 were listed in Table S5 and Table S6. Moreover, the Fig. S13 (b, d) shows the intrinsic reaction coordinate (IRC) spectra, which are utilized to confirm the accuracy of TS1 and TS2.

The IRC path indicated that the TS state was situated at the highest energy point, with 21 energy points in the optimized path. Moreover, the TS possessed the highest energy in the IRC spectra, indicating the validity of TS. The energy state of CQ combined with water through a hydrogen bond was considered zero point of energy and the different forms of CQ combined with water was computed, using the program ran

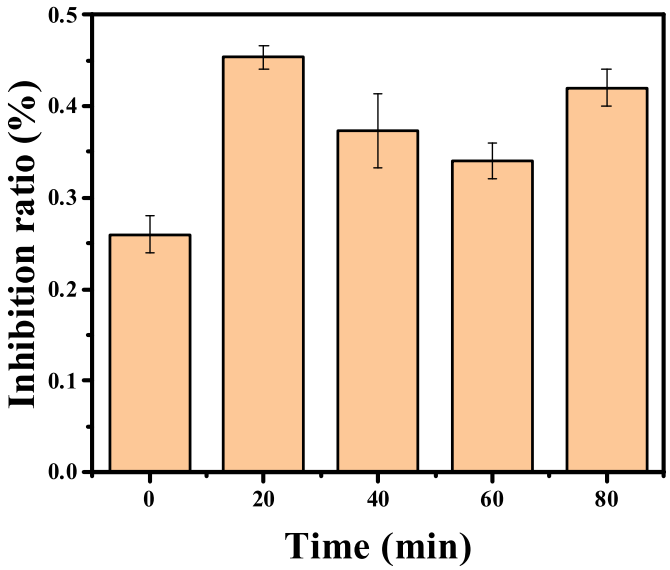

Fig. 6. The toxicity of photoproducts in CQ photodegradation process towards *Vibrio fischeri*.

by M06-2X/def2svp program (Mu et al., 2021). The hydrogen bond forms (HCQ1 and HCQ2) between CQ and H_2O were computed and presented in Fig. S14. The H_2O connected with the N on the CQ molecular to form the $H_2O\cdots H$ and $H–O–H\cdots N$ (Mu et al., 2021). The energy of HCQ1 and HCQ2 was 11.50 kJ mol^{-1} and 3.92 kJ mol^{-1} compared to the zero point of energy, respectively, demonstrating that the hydrogen bond was more stable in HCQ2 than that in HCQ1. Therefore, HCQ1 was more sensitive under solar irradiation. In Fig. 7, the energies barriers between HCQ1 and TS (1, 2) were 40.16 and 40.47 kJ mol^{-1}. The energies barriers between C2 with hydrochloric acid (HCl) and TS (1, 2) were 52.34 and 52.65 kJ mol^{-1}. Similarly, the energies barriers between HCQ2 and HCQ1 were 15.41 kJ mol^{-1}. The energy of C2 with HCl to TS (1, 2) was higher than that of HCQ1 and lower than that of HCQ2. Hence, the proposed transfer process HCQ1 → TS (1, 2) → CQOH + HCl occurred at a high reaction ratio compared with HCQ2 → TS (1, 2) → CQOH + HCl during the dechlorination of CQ.

4. Conclusions

CQ has been used in the treatment of moderate cases of COVID-19 and malaria. CQ absorbs the simulated sunlight and is activated by it. High pH values, low CQ concentration and elevate temperature

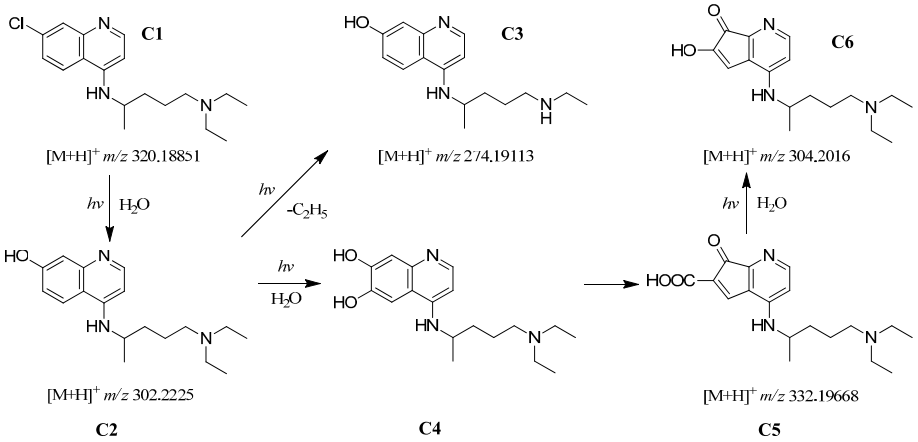

Fig. 5. The photoproducts and proposed photodegradation pathway of CQ.

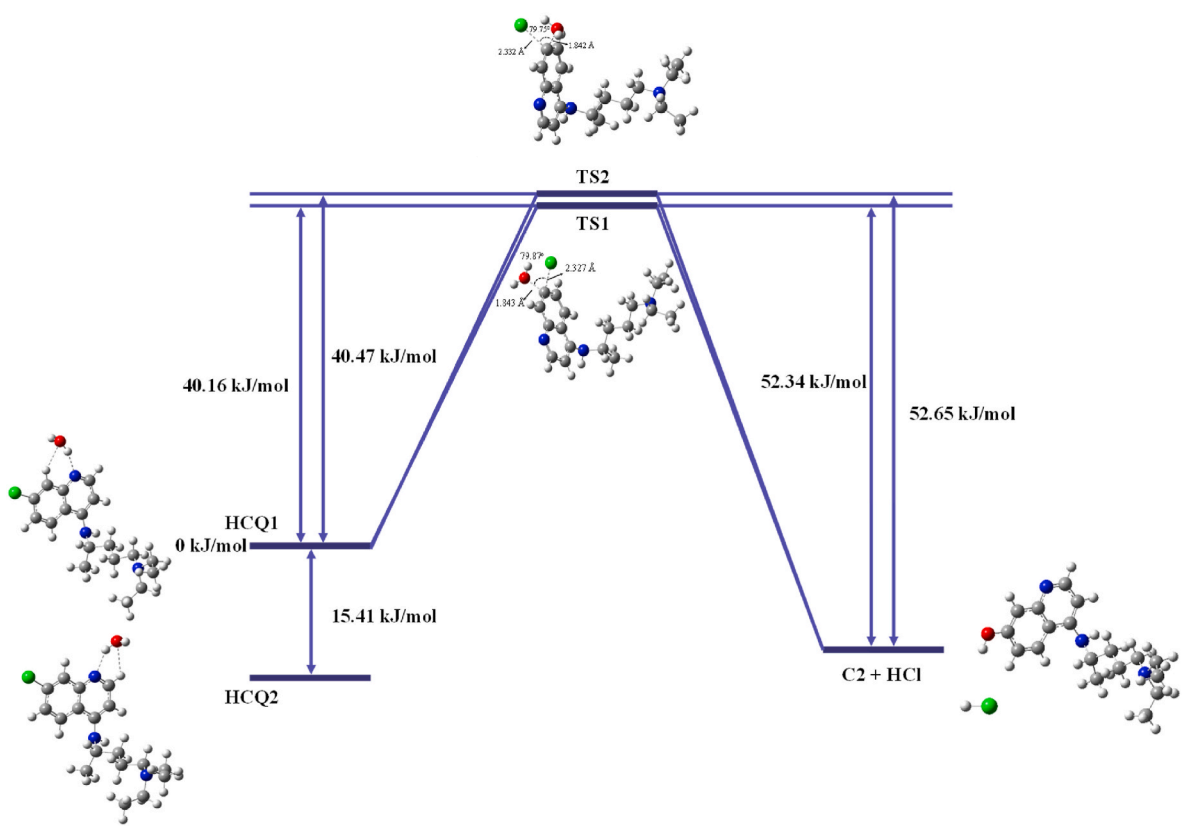

Fig. 7. The energy barrier of the dechlorination and substitution of the hydroxyl group.

exhibited positive effect on CQ photodegradation, while HA, FA and DOM in lakes exhibited negative effect on CQ photodegradation. The common cations and anions play a negligible role in the CQ photodegradation under simulated sunlight. ESR spectra, quenching experiment and probe experiment data demonstrated that the ^{3}CQ* was crucial in the CQ photodegradation processes. The photodegradation pathway of CQ was analyzed by HPLC-MS/MS and DFT calculation, revealing that C–Cl bond breaking was the first and dominant step in the CQ photodegradation process. Generally, the photoproducts toxicity towards *Vibrio fischeri* bacteria increased during CQ photodegradation process. Finally, the results provided a possible mechanism of CQ migration and transformation in the environment, supporting the elimination of other pharmaceuticals and personal care products (PPCPs) during the COVID-19 pandemic.

Declaration of competing interest

The authors declare that they have no known competing financial interests or personal relationships that could have appeared to influence the work reported in this paper.

Data availability

Data will be made available on request.

Acknowledgments

This work was supported by the National Natural Science Foundation of China (21876056, 21677054 and 22106050).

Appendix A. Supplementary data

Supplementary data to this article can be found online at https://doi.org/10.1016/j.chemosphere.2023.139093.

References

Albini, A., Monti, S., 2003. Photophysics and photochemistry of fluoroquinolones. Chem. Soc. Rev. 32, 238–250.
Anaya-Gonzalez, C., Soldevila, S., Garcia-Lainez, G., Bosca, F., Andreu, I., 2019. Chemical tuning for potential antitumor fluoroquinolones. Free Radic. Biol. Med. 141, 150–158.
Bai, Y., Zhou, Y.L., Che, X.W., Li, C.H., Cui, Z.G., Su, R.G., Qu, K.M., 2021. Indirect photodegradation of sulfadiazine in the presence of DOM: effects of DOM components and main seawater constituents. Environ. Pollut. 268.
Boreen, A.L., Edhlund, B.L., Cotner, J.B., McNeill, K., 2008. Indirect photodegradation of dissolved free amino acids: the contribution of singlet oxygen and the differential reactivity of DOM from various sources. Environ. Sci. Technol. 42, 5492–5498.
C. Bwab, C. Waa, A. Lm, Photolysis of Atrazine: Role of Triplet Dissolved Organic Matter and Limitations of Sensitizers and Quenchers, Water Research, 190.
Chen, J.W., Peijnenburg, W., Quan, X., Yang, F.L., 2000. Quantitative structure-property relationships for direct photolysis quantum yields of selected polycyclic aromatic hydrocarbons. Sci. Total Environ. 246, 11–20.
Chen, J.W., Quan, X., Yan, Y., Yang, F.L., Peijnenburg, W., 2001a. Quantitative structure-property relationship studies on direct photolysis of selected polycyclic aromatic hydrocarbons in atmospheric aerosol. Chemosphere 42, 263–270.
Chen, J.W., Quan, X., Peijnenburg, W., Yang, F.L., 2001b. Quantitative structure-property relationships (QSPRs) on direct photolysis quantum yields of PCDDs. Chemosphere 43, 235–241.
Chen, Y., Li, H., Wang, Z., Tao, T., Wei, D., Hu, C., 2012. Photolysis of chlortetracycline in aqueous solution: kinetics, toxicity and products. J. Environ. Sci. 24, 254–260.
Chen, Y., Liu, L., Su, J., Liang, J.F., Wu, B., Zuo, J.L., Zuo, Y.G., 2017. Role of humic substances in the photodegradation of naproxen under simulated sunlight. Chemosphere 187, 261–267.
Cheng, K., Zhang, L., McKay, G., 2023. Evaluating the Microheterogeneous Distribution of Photochemically Generated Singlet Oxygen Using Furfuryl Amine. Environmental science & technology.
Dabic, D., Hanzevacki, M., Skoric, I., Zegura, B., Ivankovic, K., Biosic, M., Tolic, K., Babic, S., 2022. Photodegradation, Toxicity and Density Functional Theory Study of Pharmaceutical Metoclopramide and its Photoproducts. Science of the Total Environment, p. 807.
Du, Y.X., Chen, X.P., 2020. Favipiravir: pharmacokinetics and concerns about clinical trials for 2019-ncov infection. Clin. Pharmacol. Ther. 108, 242–247.

Gaigalas, A.K., Wang, L., Cole, K.D., Humphries, E., 2004. Photodegradation of fluorescein in solutions containing n-propyl gallate. J. Phys. Chem. A 108, 4378–4384.
Gao, J.J., Tian, Z.X., Yang, X., 2020. Breakthrough: chloroquine phosphate has shown apparent efficacy in treatment of COVID-19 associated pneumonia in clinical studies. Bioscience Trends 14, 72–73.
Ge, L.K., Chen, J.W., Wei, X.X., Zhang, S.Y., Qiao, X.L., Cai, X.Y., Xie, Q., 2010. Aquatic photochemistry of fluoroquinolone antibiotics: kinetics, pathways, and multivariate effects of main water constituents. Environ. Sci. Technol. 44, 2400–2405.
Janssen, E.M.L., Erickson, P.R., McNeill, K., 2014. Dual roles of dissolved organic matter as sensitizer and quencher in the photooxidation of tryptophan. Environ. Sci. Technol. 48, 4916–4924.
Kulovaara, M., Corin, N., Backlund, P., Tervo, J., 1996. Impact of UV-254-radiation on aquatic humic substances. Chemosphere 33, 783–790.
Makunina, M.P., Pozdnyakov, I.P., Chen, Y., Grivin, V.P., Bazhin, N.M., Plyusnin, V.F., 2015. Mechanistic study of fulvic acid assisted propranolol photodegradation in aqueous solution. Chemosphere 119, 1406–1410.
Mathon, B., Coquery, M., Miege, C., Vandycke, A., Choubert, J.M., 2019. Influence of water depth and season on the photodegradation of micropollutants in a free-water surface constructed wetland receiving treated wastewater. Chemosphere 235, 260–270.
Mu, Y., Chen, Y., Chen, P., Qin, L.M., Zou, J.P., Wu, M.F., Luo, S.L., 2021. New insights into the degradation of atrazine by ultraviolet-based techniques. Acs Es&T Water 1, 958–968.
Redman, Z.C., Wesolowski, J., Tomco, P.L., 2021. Photochemical pathways of rotenone and deguelin degradation: implications for rotenoid attenuation and persistence in high-latitude lakes. Environ. Sci. Technol. 55, 4974–4983.
Remke, S.C., Burgin, T.H., Ludvikova, L., Heger, D., Wenger, O.S., von Gunten, U., Canonica, S., 2022. Photochemical Oxidation of Phenols and Anilines Mediated by Phenoxyl Radicals in Aqueous Solution. Water Research, p. 213.
Simani, L., Ramezani, M., Darazam, I.A., Sagharichi, M., Aalipour, M.A., Ghorbani, F., Pakdaman, H., 2021. Prevalence and correlates of chronic fatigue syndrome and post-traumatic stress disorder after the outbreak of the COVID-19. J. Neurovirol. 27, 154–159.
Snyrychova, I., Hideg, E., 2007. The first application of terephthalate fluorescence for highly selective detection of hydroxyl radicals in thylakoid membranes. Funct. Plant Biol. 34, 1105–1111.
Song, Q.H., Lin, W.Z., Yao, S.D., Lin, N.Y., 1998. Comparative studies of triplet states of thymine components by acetone sensitization and direct excitation in aqueous solution at room temperature. J. Photochem. Photobiol. A Chem. 114, 181–184.
Sulistyaningrum, N., Arlinda, D., Hutagalung, J., Sunarno, S., Oktoberia, I.S., Handayani, S., Ekowatiningsih, R., Yusnita, E.A., Prasetyorini, B., Rizki, A., Tjitra, E., Na-Bangchang, K., Chaijaroenkul, W., 2020. Prevalence of glucose 6-phosphate dehydrogenase variants in malaria-endemic areas of south central timor, eastern Indonesia. Am. J. Trop. Med. Hyg. 103, 760–766.
Wan, D., Kong, Y., Wang, X., Selvinsimpson, S., Sharma, V.K., Zuo, Y., Chen, Y., 2022a. Effect of Permanganate Oxidation on the Photoreactivity of Dissolved Organic Matter for Photodegradation of Typical Pharmaceuticals. Science of the Total Environment, p. 813.
Wan, D., Wang, J., Chen, T., Xiang, W., Selvinsimpson, S., Chen, Y., 2022b. Effect of Disinfection on the Photoreactivity of Effluent Organic Matter and Photodegradation of Organic Contaminants. Water Research, p. 219.
Wang, S., Song, X.D., Hao, C., Gao, Z.X., Chen, J.W., Qiu, J.S., 2015. Elucidating triplet-sensitized photolysis mechanisms of sulfadiazine and metal ions effects by quantum chemical calculations. Chemosphere 122, 62–69.
Wang, M.L., Cao, R.Y., Zhang, L.K., Yang, X.L., Liu, J., Xu, M.Y., Shi, Z.L., Hu, Z.H., Zhong, W., Xiao, G.F., 2020. Remdesivir and chloroquine effectively inhibit the recently emerged novel coronavirus (2019-nCoV) in vitro. Cell Res. 30, 269–271.
Wenk, J., von Gunten, U., Canonica, S., 2011. Effect of dissolved organic matter on the transformation of contaminants induced by excited triplet states and the hydroxyl radical. Environ. Sci. Technol. 45, 1334–1340.
Yao, X.T., Ye, F., Zhang, M., Cui, C., Huang, B.Y., Niu, P.H., Liu, X., Zhao, L., Dong, E.D., Song, C.L., Zhan, S.Y., Lu, R.J., Li, H.Y., Tan, W.J., Liu, D.Y., 2020. In vitro antiviral activity and projection of optimized dosing design of hydroxychloroquine for the treatment of Severe Acute Respiratory Syndrome Coronavirus 2 (SARS-CoV-2). Clin. Infect. Dis. 71, 732–739.
Yi, X.H., Ji, H.D., Wang, C.C., Li, Y., Li, Y.H., Zhao, C., Wang, A.O., Fu, H.F., Wang, P., Zhao, X., Liu, W., 2021. Photocatalysis-activated SR-AOP over PDINH/MIL-88A(Fe) Composites for Boosted Chloroquine Phosphate Degradation: Performance, Mechanism, Pathway and DFT Calculations. Applied Catalysis B-Environmental, p. 293.
Yu, Y., Zhou, D., Wu, F., 2015. Mechanism and products of the photolysis of hexabromocyclododecane in acetonitrile–water solutions under a UV-C lamp. Chem. Eng. J. 281, 892–899.
Zhang, S.Y., Chen, J.W., Zhao, Q., Xie, Q., Wei, X.X., 2016. Unveiling self-sensitized photodegradation pathways by DPT calculations: a case of sunscreen p-aminobenzoic acid. Chemosphere 163, 227–233.
Zhang, X., Li, J., Fan, W.Y., Yao, M.C., Yuan, L., Sheng, G.P., 2019a. Enhanced photodegradation of extracellular antibiotic resistance genes by dissolved organic matter photosensitization. Environ. Sci. Technol. 53, 10732–10740.
Zhang, Z., Xie, X., Yu, Z., Cheng, H., 2019b. Influence of chemical speciation on photochemical transformation of three fluoroquinolones (FQs) in water: kinetics, mechanism, and toxicity of photolysis products. Water Res. 148, 19–29.
Zhao, D.H., Yao, F.F., Wang, L.J., Zheng, L., Gao, Y.J., Ye, J., Guo, F., Zhao, H., Gao, R.B., 2020. A comparative study on the clinical features of Coronavirus 2019 (COVID-19) pneumonia with other pneumonias. Clin. Infect. Dis. 71, 756–761.
Zhou, L., Ji, Y.F., Zeng, C., Zhang, Y., Wang, Z.Y., Yang, X., 2013. Aquatic photodegradation of sunscreen agent p-aminobenzoic acid in the presence of dissolved organic matter. Water Res. 47, 153–162.